Surface Synthesis of Zinc Sulfide Nanoparticles on Silica Microspheres: Sonochemical Preparation, Characterization, and Optical Properties

N. Arul Dhas, A. Zaban, and A. Gedanken*

Department of Chemistry, Bar-Ilan University, Ramat-Gan, 52900 Israel

Received September 24, 1998. Revised Manuscript Received December 17, 1998

Ultrasonic irradiation of a slurry of amorphous silica microspheres, zinc acetate, and thioacetamide in an aqueous medium for 3 h under ambient air yields zinc sulfide coated on silica. The powder X-ray diffraction of the initial zinc sulfide−silica (ZSS) powder yields diffraction peaks corresponding to the ZnS phase. The TEM image of ZSS shows that the porous ZnS nanoparticles (diameter 1−5 nm) coated the silica (SiO_2) surface as thin layers or nanoclusters, depending on the reactant concentration. Infrared spectroscopy illustrates the structural changes that occurred in the siloxane network and surface silanol groups of SiO_2 upon the ultrasonic deposition of ZnS. The optical absorption of porous ZnS shows a broad band at around 610 nm, ascribed to unusual surface state transition. The absorption energy of the surface state transition is lower than the band gap of the ZnS particles and probably stems from the dangling surface bonds or defects. On the other hand, the ZSS does not show the surface state transition of ZnS, probably due to the strong surface interaction with SiO_2. The classical valence-conduction transition band has been observed in the optical reflectance mode, and it shows an absorption edge at around (290−310 nm), which is markedly blue-shifted compared to that of bulk ZnS (345 nm). The photoluminescence spectrum of the porous ZnS and ZSS shows a band with a maximum centered around 420 nm, which is similar to that of quantum ZnS particles. We propose that the coating process takes place via ultrasonic-cavitation-induced initial grafting of zinc acetate onto the silica surface, followed by the displacement of acetate ion by in situ generated S^{2-} species.

1. Introduction

Semiconductor nanoparticles have been extensively studied from experimental and theoretical viewpoints, owing to their potential applications in solar energy conversion, photocatalysis, and optoelectronic industry that stem from their size-dependent optical properties.[1−8] This is associated with the quantum size effect and with the existence of a relatively large percentage of atoms at the surface. Nowadays, many synthetic routes have been developed to control the size and distribution of the semiconductor nanoparticles. However, thermal treatment is necessary in some of the methods, and this is not favorable for the production of quantum-sized semiconductor particles with large surface atoms.

One of the most advanced and intriguing developments in the area of nanoparticles is the coating of semiconductor clusters on a solid support.[4−8] This can be exploited to synthesize core/shell type materials with unique optical, electronic, magnetic, and catalytic properties that are more than the sum of their individual components. Although the technology for coating the nanoparticles on rather large substrates is well-established, coating on very small substrates, such as submicron-sized particles, still remains a technical challenge. The coating of semiconductor nanoclusters has been accomplished using either of the two following strategies: (i) the transfer of solution phase synthesized semiconductor nanoclusters to a desired core substrate and further thermal treatment to obtain the core/shell material[4] and (ii) the surface or the direct synthesis of semiconductor nanoclusters on a solid support.[5] The surface synthesis has frequently involved the deposition of a material using either molecular beam epitaxy or chemical vapor deposition. The epitaxial electrochemical deposition of semiconductor nanocrystallites was accomplished for the first time by Hodes, Rubinstein, and co-workers.[5]

Currently, considerable efforts have been made to bind semiconductor nanoclusters to metal surfaces using a self-assembled monolayer approach or by synthesizing multilayered metal nanoclusters. Kamat and Shanghavi[6] have studied the optical properties of semiconductor/metal composite prepared by the self-assembled

* Corresponding author. E-mail: gedanken@mail.biu.ac.il. Fax: + 972 -3-5351250.

(1) Henglein, A. *Ber. Bunsen-Ges. Phys. Chem.* **1995**, *99*, 903. Spanhel, L.; Hnase, M.; Weller, H.; Henglein, A. *J. Am. Chem. Soc.* **1987**, *109*, 5649.
(2) Brus, L. E. *J. Phys. Chem.* **1983**, *79*, 5556; **1984**, *80*, 4403; **1986**, *90*, 2555.
(3) Wang, Y.; Herron, N. *J. Phys. Chem.* **1987**, *91*, 257. Petit, C. Pileni, M. P. *J. Phys. Chem.* **1988**, *92*, 2282.
(4) Colvin, V. L.; Schlamp, M. C.; Alivisatos, A. P. *Nature* **1994**, *370*, 354.
(5) Golan, Y.; Margulis, L.; Hodes, G.; Rubinstein, I.; Hutchinson, J. L. *Surf. Sci.* **1994**, *311*, L633.
(6) Kamat, P. V.; Shanghavi, B. *J. Phys. Chem.* **1997**, *101*, 7675.
(7) Peng, X.; Schlamp, M. C.; Kadavanich, A. V.; Alivisatos, A. P. *J. Am. Chem. Soc.* **1997**, *119*, 7019.
(8) Kortan, A. R.; Hull, R.; Opila, R. L. Bawendi, M. G.; Steigerwald, M. L.; Carroll, P. J.; Brus, L. E. *J. Am. Chem. Soc.* **1990**, *112*, 1327.

10.1021/cm980670s CCC: $18.00
Published on Web 02/25/1999

monolayer approach. Alivisatos et al.[7] have synthesized luminescent semiconductor core/shell nanocrystals using a two-dimensional artificial structure growth, i.e., epitaxial growth. Brus and co-workers[8] have studied the nucleation and growth of CdSe on ZnS and ZnS on CdSe quantum crystallite seeds in an inverse micelle media.

Recently, sonochemical processing has been proven to be a useful technique for generating novel materials with unusual properties.[9] The chemical effects of ultrasound arise from acoustic cavitation, that is, the formation, growth, and implosive collapse of bubbles in liquid. The implosive collapse of the bubble generates localized hot spots through adiabatic compression or shock wave formation within the gas phase of the collapsing bubble. The conditions formed in these hot spots have been experimentally determined, with transient temperatures of ~5000 K, pressures of 1800 atm, and cooling rates in excess of 10^8 K/s. These extreme conditions attained during bubble collapse have been exploited to prepare amorphous metals,[10] carbides,[11] oxides,[12] sulfides,[13] and composite[14] nanoparticles. In the present work, we report for the first time on the surface synthesis of ZnS semiconductor nanoparticles on submicron-sized SiO_2 by the ultrasound irradiation of a slurry of SiO_2, zinc acetate, and thioacetamide in water, at near room temperature. We have also focused our attention on the reaction mechanism of ZSS formation under the given sonochemical conditions. Characterization was accomplished using various techniques, such as powder X-ray diffraction, energy-dispersive X-ray analysis, transmission electron microscopy, infrared spectroscopy, optical absorption and reflectance, and photoluminescence spectroscopy.

2. Experimental Section

Materials. Zinc acetate [$Zn(ac)_2$] and thioacetamide (TA) were purchased from Aldrich and used without further purification. SiO_2 was prepared by base hydrolysis and condensation of tetraethyl orthosilicate in an aqueous ethanol medium containing ammonia.[15] The silica was thermally pretreated at 700 °C for 4 h, leaving the surface covered exclusively with silanols. Doubly distilled water was used for the sonication. Ultrasonic irradiation was accomplished with a high-intensity ultrasonic probe (Misonix, XL sonifier, 1.13 cm diameter Ti horn, 20 kHz, 100 Wcm^{-2}). A round-bottom Pyrex glass vessel (total volume ~100 mL) was used for the ultrasound irradiation, which was carried out under ambient air. The sonochemical synthesis of ZnS was described in great detail by Grieser and co-workers,[13] we have followed their procedure. The method of preparation will not be repeated herein. We will, however outline the preparation of ZSS.

Table 1. Reactant Composition and Sonochemical Reaction Conditions Employed for the Sonochemical Coatings of Silica

sample code	amount (mg)			sonication time (h)	bulk temp ± 5 (°C)
	silica	$Zn(ac)_2$	RS		
ZnS		600	200	3	80
ZSS	100	600	200	3	80
ZSS−C1	100	300	100	2	80
ZSS−C2	100	100	34	2	80

Scheme 1

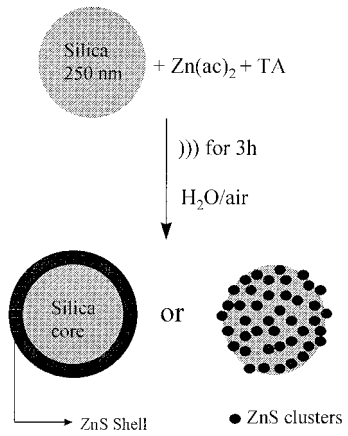

Surface Synthesis of ZnS on SiO_2. Ultrasonic irradiation of a stoichiometric ratio of $Zn(ac)_2$, TA, and SiO_2 in an aqueous medium yields a ZnS-coated SiO_2 composite. On the other hand, in contrast to the use of $Zn(ac)_2$, zinc nitrate, zinc chloride or zinc perchlorate solutions did not show the coating behavior of the resulting ZnS on silica. Therefore, the choice of the Zn^{2+} ion source seems to be a particularly important factor for the sonochemical surface synthesis of ZnS. The reactant composition and the experimental parameters for the sonochemical preparation of ZnS and ZSS are summarized in Table 1. The schematic representation for the sonochemical formation of ZSS with different surface morphology is given in Scheme 1.

Typically, for the preparation of ZSS, a slurry of $Zn(ac)_2$ (600 mg), TA (200 mg), and SiO_2 (100 mg) in 100 mL of distilled water was sonicated with a high-intensity ultrasonic horn (direct immersion) at room temperature for 3 h, under ambient air. The temperature of the reaction mixture rose to 80 °C during the ultrasonic irradiation. The resulting white powder was recovered by centrifugation, washed repeatedly with distilled water and ethanol, and then dried in a vacuum.

We have tried to synthesize ZSS under the same experimental conditions, without making use of the ultrasound radiation. This however, did not yield ZSS. This indicates that the ultrasound plays an important role in the formation and coating of ZnS on the SiO_2 carrier.

Characterization. The phase composition and nature of the ZSS was determined by X-ray diffraction (XRD), using a Rigaku 2028, CuKα diffractometer. Domain size was calculated from the X-ray line broadening, using the Debye−Scherrer equation.[16] The energy-dispersive X-ray (EDX) analysis of the ZSS was carried out to ascertain the chemical composition, using a JEOL-JSM-840 electron microscope. The overall morphologies of the ZnS and ZSS were obtained by transmission electron microscopy (TEM), using a JEOL-JEM 100SX electron microscope. Samples for the TEM measurements were obtained by placing a drop of sample suspension in dioxane on a carbon-coated Formvar copper grid (400 mesh, Electron Microscopy Sciences), followed by air-drying to remove the solvent. Infrared spectra were recorded using a Nicolet (Impact 410) FT-IR spectrometer, using transparent

(9) *Ultrasound: Its Chemical, Physical and Biological Effects*; Suslick, K. S., Ed.; VCH: Weinheim, 1988.

(10) Suslick, K. S.; Choe, S. B.; Cichowlas, A. A.; Grinstaff, M. W. *Nature* **1991**, *353*, 414. Aul Dhas, N.; Paul Raj. P.; Gedanken, A. *Chem. Mater.* **1998**, *10*, 1446. Arul Dhas, N.; Cohen, H.; Gedanken, A. *J. Phys. Chem.* **1997**, *101*, 6834.

(11) Hyeon, T.; Fang, M.; Suslick, K. S. *J. Am. Chem. Soc.* **1996**, *118*, 5492.

(12) Cao, X.; Koltypin, Y.; Katabi, G.; Felner, I.; Gedanken, A. *J. Mater. Res.* **1997**, *12*, 405. Arul Dhas, N.; Kotypin, Y.; Gedanken, A. *Chem. Mater.* **1997**, *9*, 3159.

(13) Sostaric, J. Z.; Caruso-Hubson, R. A.; Mulvaney, P.; Grieser, F. *J. Chem. Soc., Faraday Trans.* **1997**, *93*, 1791.

(14) Arul Dhas, N.; Gedanken, A. *J. Phys. Chem.* **1997**, *101*, 9495. Arul Dhas, N.; Gedanken, A. *Chem. Mater.* **1997**, *9*, 3144. Arul Dhas, N.; Gedanken, A. *Appl. Phys. Lett.* **1998**, *72*, 2511.

(15) Stober, W.; Fink, A.; Bohn, E. *J. Colloid Interface Sci.* **1968**, *26*, 62.

(16) *X-ray Diffraction Procedures*; Klug, H., Alexander L., Eds.; Wiley: New York, 1962; p 125.

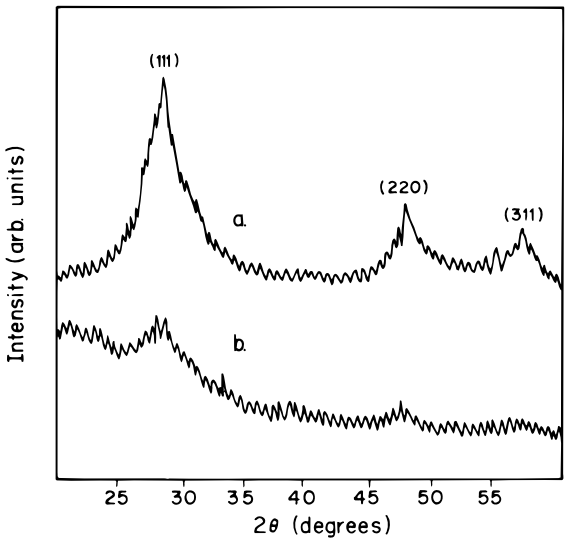

Figure 1. Powder XRD patterns: (a) ZnS and (b) ZSS.

pellets of the compounds in KBr (Aldrich, FT-IR grade) matrices. KBr was used as the background file. All spectra were measured from approximately 4000 to 400 cm^{-1}, and the number of scans was typically 75, with a resolution of 4 cm^{-1}. The reflectance and direct UV−visible absorption spectra of the ZnS and ZSS were recorded on a Cary (varian 1E) spectrophotometer. The photoluminescence (PL) spectrum was obtained using a Perkin-Elmer luminescence spectrophotometer (model LS50B). The excitation wavelength was 290 nm. The solid ZnS and ZSS powders were uniformly cast on a glass plate as a thin film, using ethanol for the UV−visible and PL measurements.

3. Results

Powder XRD and EDX Studies. The XRD pattern of ZnS shows the presence of broad peaks (Figure 1a), corresponding to the zinc blende crystal structure. The three diffraction peaks correspond to the (111), (220), and (311) planes of the cubic crystalline ZnS. The domain size of the particles estimated from the Debye−Scherrer formula is 1.4 nm. The diameter of the sonochemically produced bare ZnS is much smaller than the Bohr radius of ZnS (2.5 nm).[17] The XRD profile of the ZSS (Figure 1b) shows the presence of weak diffraction peaks. The peak positions of ZSS matches with the bare ZnS nanoparticles. The presence of weak XRD peaks in the ZSS sample can be attributed to the partial crystalline nature of ZnS and/or to the small amount of ZnS (13.4%, determined using EDX, see below). The observed rising background in the lower angle side ($2\theta \sim 22°$) is due to the presence of the amorphous SiO_2 core.

The EDX pattern (Figure 2a) for the ZnS shows the presence of Zn and S peaks. The appearance of a small O peak in the lower energy side presumably originates from the trapped acetate or solvent molecules as well. This was further confirmed by the IR measurements. The calculated ratio of the amount of Zn and S elements, using EDX peak intensity, was 25−18.6, respectively. The EDX profile of the ZSS (Figure 2b) shows the additional signal corresponding to Si and O elements, apart from the ZnS signals, where the ratio of Zn:S was 11:9. EDX is not considered a precise method, particularly when a nonplanar surface is involved; we therefore hesitate to claim that the Zn:S molar ratio is deviating from 1.

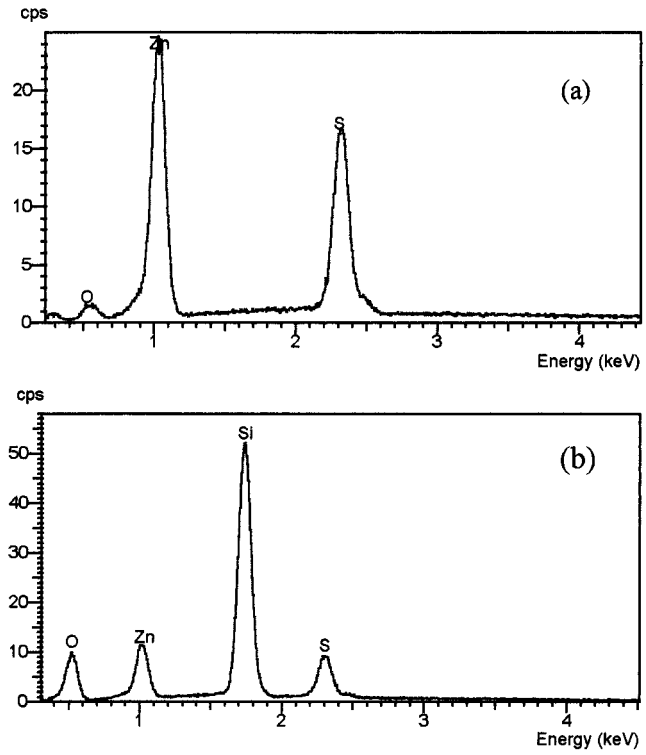

Figure 2. EDX profiles: (a) ZnS and (b) ZSS.

TEM Studies. The TEM micrograph of bare ZnS (Figure 3a) shows the presence of irregularly shaped fine particles. The particles are held together by a porous irregular network. The average size of these nanoparticles is in the range of 1−5 nm. TEM images of the ZSS, with different concentrations of ZnS (Figure 3b−d), reveal the coating nature of the ZnS nanoparticles. It can be seen that the ZnS nanoparticles generated by the sonochemical conditions are coated on the surface of SiO_2 (250 nm diameter). The SiO_2 spheres are almost uniformly coated with ZnS, without any free bare zones. In ZSS (Figure 3b), the central SiO_2 core is coated with a regular periphery of ZnS layers of approximately 10 nm thickness. An interesting point to be mentioned here is that we did not observe the presence of free SiO_2 or ZnS particles in the ZSS composite. However, when the concentration of ZnS is increased, a collection of free ZnS nanoparticles has been observed. The TEM image of the ZSS−C1 (Figure 3c) and ZSS−C2 (Figure 3d) reveals that the ZnS nanoparticles are coated on the surface of SiO_2 as clusters (size ~20 nm), not as the thin layer structure shown by ZSS. Almost all of the SiO_2 spheres were coated by the clusters of ZnS nanoparticles.

Infrared Studies. The IR spectrum of the bare silica spheres can be found in refs 14 and 18 and will not be repeated in this report. Infrared (IR) spectra of the SiO_2 and ZSS (Figure 4) clearly show the formation of an interfacial bond between SiO_2 and ZnS. The IR spectrum of the SiO_2 shows (Figure 4a) three absorption bands in the region of 1600−400 cm^{-1}, characteristic of

(17) Rossetti, R.; Hull, R.; Gibson, J. M.; Brus, L. E. *J. Chem. Phys.* **1985**, *82*, 552.

(18) Kirk, C. T. *Phy. Rev. B* **1988**, *38*, 1255. Hu, S. M. *J. Appl. Phys.* **1980**, *51*, 5945.

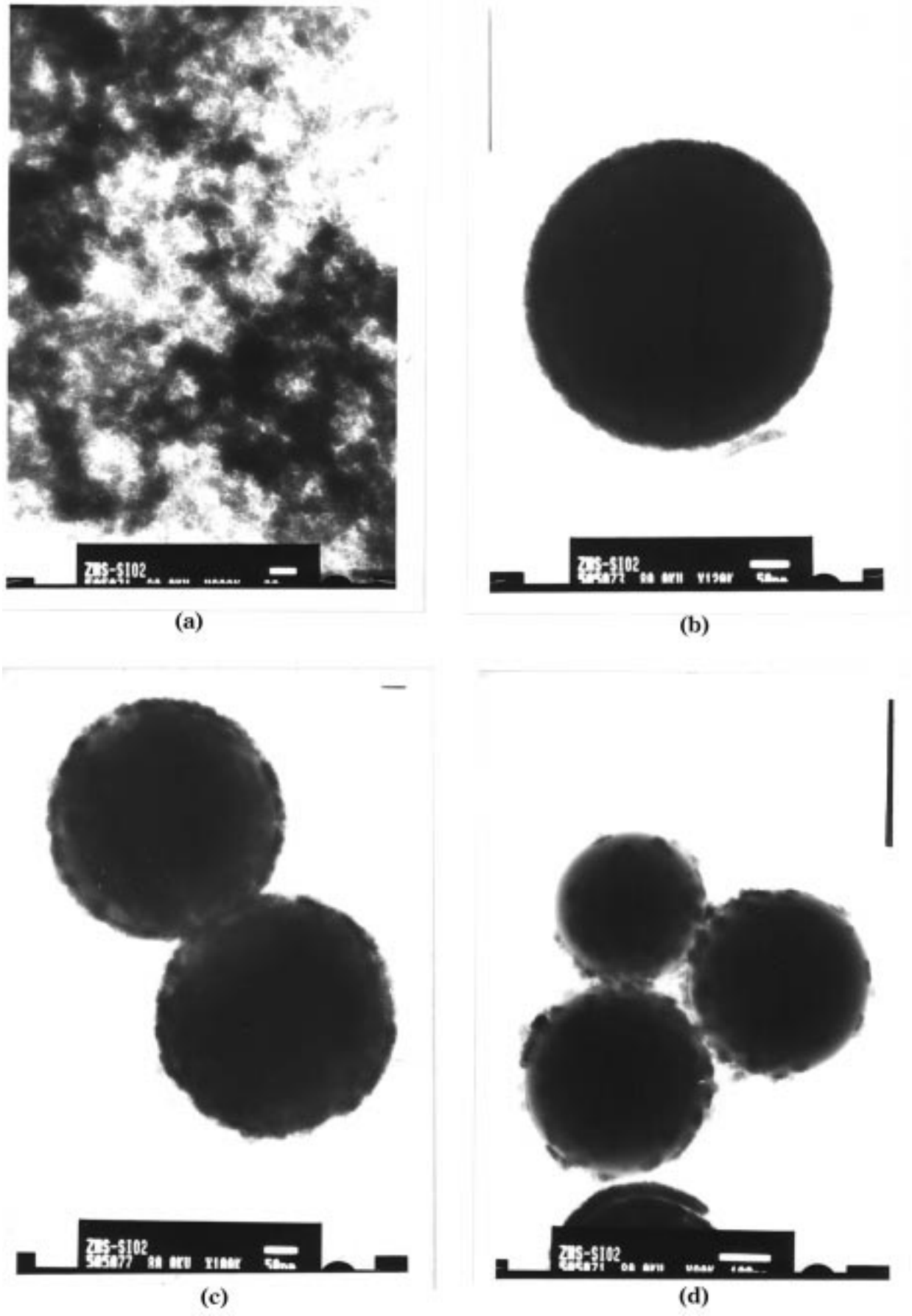

Figure 3. TEM micrographs: (a) ZnS (bar = 20 nm), (b) ZSS (bar = 50 nm), (c) ZSS−C1 (bar = 50 nm), and (d) ZSS−C2 (bar = 100 nm).

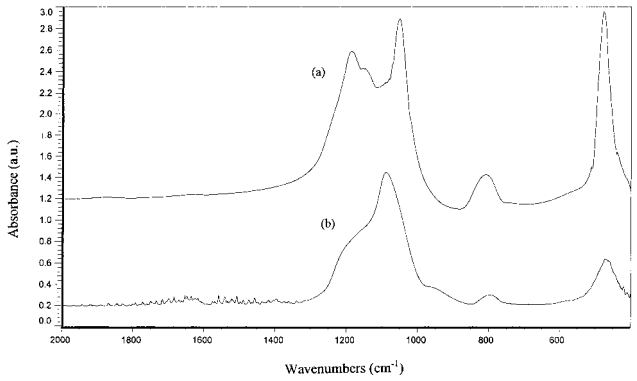

Figure 4. FT-IR spectra: (a) SiO_2 and (b) ZSS composite.

the siloxane links.[18] The absorption band at ~460 cm^{-1} corresponds to the racking mode, while the band at ~810 cm^{-1} is due to the symmetric stretching of the Si−O−Si group.[18] The observed broad doublet band in the wavenumber region of 1300−900 cm^{-1} corresponds to the asymmetric stretching (AS) vibrational mode of the Si−O−Si bridge of the siloxane link. The sharp band at 1060 cm^{-1} corresponds to the characteristic oxygen asymmetric stretch mode (AS). The splitting of the AS mode of the SiO_2 is probably due to the presence of strained siloxane links and surface silanols (disorder-induced coupling), as recognized earlier.[14,19]

The IR spectrum of the ZSS (Figure 4b) shows a significant change in the AS mode of the SiO_2 core. The doublet of the SiO_2 AS band was replaced by a sharp band near 1120 cm^{-1}, corresponding to the AS mode and indicating a surface modification of the ZnS coating by ultrasonic cavitation. A higher frequency shift of 60 cm^{-1} was observed for the AS mode upon coating, probably associated with the bonding change around the [SiO_4] tetrahedra. The splitting of the AS mode of SiO_2 disappeared upon sonochemical deposition of the ZnS on the SiO_2 surface. However, a less intense small shoulder in the region of 1200 cm^{-1} could still be detected, typifying a low degree of disorder splitting, due to the depletion of strained siloxane networks and surface silanols of amorphous SiO_2 upon sonochemical coating. Thus, the decreased intensity of the splitting of the AS mode reveals surface ordering by breaking the strained siloxane networks and the silanols of the SiO_2 upon ultrasound cavitation. A similar kind of surface modification of the silica core was observed for other systems.[14] The above results demonstrate that the ultrasound-induced cavitation appears to play a dual role, that is, in the decomposition of thioacetamide to generate ZnS and in the activation of the SiO_2 surface for the adhesion of the resulting ZnS species.

Optical Properties. *Absorption Spectra.* The room-temperature optical absorption spectrum of ZnS and ZSS is shown in Figure 5. A strong absorption band appearing in the direct absorption spectra of ZnS at around 610 nm can be attributed to the surface state of ZnS nanoparticles because the absorption lies below the absorption edge of the particles, i.e., the absorption energy is lower than the band gap of the particles.[20] This

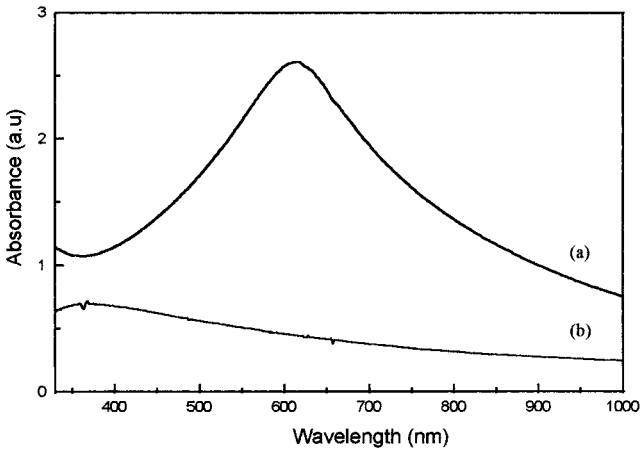

Figure 5. Optical absorption spectra: (a) ZnS and (b) ZSS.

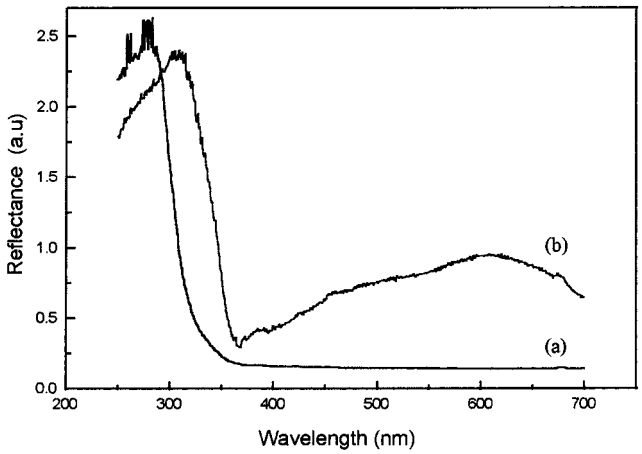

Figure 6. Optical reflectance spectra: (a) ZnS and (b) ZSS.

assignment follows the work of Tan and Zhang,[22] who have observed the same absorption peak, and their assignment is also adopted by us. The large fraction of surface atoms leads to the large number of dangling bonds and stoichiometric or external defects originating from the surface transition. The absorption in the long-wavelength region disappears totally for the ZSS powders. This is probably due to the capping of q-ZnS on SiO_2 carrier. The contents of the surface states may be largely reduced due to the charge transfer between the core and shell.

Reflectance Spectra. We have carried out the reflectance spectra of ZnS and ZSS in order to resolve the excitonic or interband (valence-conduction band) transition of ZnS, which allows us to calculate the band gap. Figure 6 shows the optical reflectance spectra of ZnS and ZSS. The very sharp drop in the reflectance spectra of ZnS and ZSS demonstrates the narrow size distribution of ZnS. The optical reflection edge of bare ZnS is 290 nm, and it is 310 nm for the ZnS in the ZSS. The absorption edges of both bare ZnS and ZSS are fairly blue-shifted from the absorption edge of the bulk ZnS (345 nm).[21] This clearly indicates the presence of quantum size effects in the sonochemically prepared ZnS nanoparticles. The small red-shift of the ZSS absorption edge, compared to that of the ZnS, can be attributed to the strong interaction between the ZnS and

(19) Gaskell, P. H.; Johnson, D. W. *J. Non-Cryst. Solids* **1976**, *20*, 153.
(20) Chen, W.; Wang, Z.; Lin, Z.; Lin, L. *J. Appl. Phys.* **1997**, *82*, 3111.
(21) *Introduction to Solid State Physics*, Kittel, C., Ed.; Wiley: New York, 1986; Chapter 8.
(22) Tan, M.; Cai, W. Zhang, L. *Appl. Phys. Lett.* **1997**, *71*, 3697.

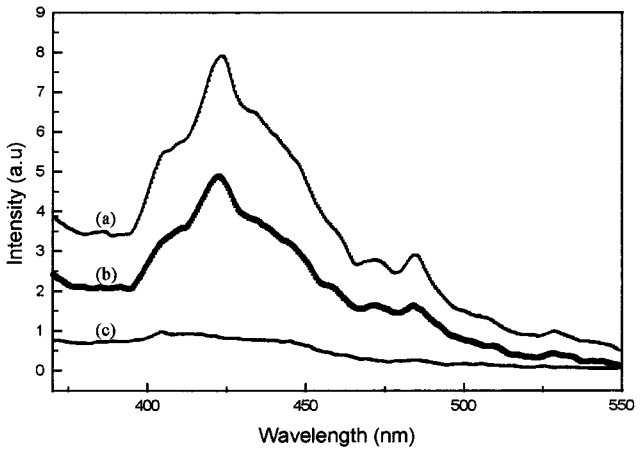

Figure 7. Photoluminescence spectra: (a) ZnS, (b) ZSS, and (c) background (glass plate). The excitation wavelength for all spectra is 290 nm.

SiO_2 and to the weakly crystalline nature of ZnS.[22] The observed small broad hump in the higher wavelength side of the reflectance spectrum of the ZSS could be due to the scattering of light by the silica core. We have calculated the band gaps of bare ZnS and ZnS in ZSS, which are 4.2 and 4.0 eV, respectively. The value of the band gap energy is also reasonably larger than that of the reported value for bulk ZnS (3.65 eV).

Photoluminescence Spectra. Figure 7 shows the PL spectra of the sonochemically generated ZnS and ZSS. No luminescence is observed above 550 nm. The PL spectra of the background glass plate spectrum is also included for comparison. The PL spectrum of the ZnS (Figure 7a) shows a broad emission band centered at 420 nm. A similar emission band peaking at 424 nm was detected by Khosravi et al.[23] for 2.1 nm sized ZnS particles. They have interpreted this emission band as originating from defect states. The observed band in our experiments can be assigned to emission from the recombination of electrons and holes in trapped surface states located in the "forbidden" region of the band gap.[24] A modest blue-shift (~20 nm) of the emission band position relative to that of the bulk ZnS (440−500 nm) is observed, which may be due to the size quantization effect of the ZnS nanocrystallites. Further, ZSS displays its emission band at around 420 nm (Figure 7b). It is evident that the broad emission feature is not from the background glass plate (Figure 7c), but rather from the ZnS. It is worth mentioning that other studies[25] have detected two blue emissions in this energy region in colloidal suspensions of ZnS. The bands were detected at 428 and 418 nm. They were assigned to a sulfur vacancy and interstitial sulfur lattice defects, respectively.[25] Early interpretations have attributed the ZnS emission to a cation vacancy whose nearest surroundings have lost one electron.[26]

Discussion

The chemical reactions driven by intense ultrasonic waves which are strong enough to produce cavitation are oxidation, reduction, dissolution, and decomposition.[9,27] Other reported reactions include the promotion of polymerization that is induced by ultrasound. It is known that three different regions are formed during the aqueous sonochemical process: (1) the inner environment (gas phase) of the collapsing bubble, where elevated temperatures (several thousands of degrees) and pressures (hundreds of atmospheres) are produced, which causes water to vaporize and further pyrolyze into $H^\bullet$ and $OH^\bullet$ radicals; (2) the interfacial region between the cavitation bubbles and the bulk solution, where the temperature is lower than in the gas-phase region but still high enough to induce a sonochemical reaction; and (3) the bulk solution, which is at ambient temperatures and is where the reaction between reactant molecules and the formed radicals takes place. Among the above-mentioned three regions, it appears that the interfacial zone and the bulk solution are the major areas in which the sonochemical reaction takes place. Due to the low vapor pressure of the reactants (SiO_2, thioacetamide, and zinc acetate), only a negligible amount of formation and coating of ZnS is expected to occur in the cavity or bubble. On the basis of a comparison with radiation chemistry studies,[13,27] the reactions occurring during sonication which lead to ZnS formation are believed to be:

$$H_2O))))) \; H^\bullet + OH^\bullet \tag{1}$$

$$2H^\bullet + RS \rightarrow H_2S + R^\bullet \quad (RS = \text{thioacetamide}) \tag{2}$$

$$H_2S + Zn(Ac)_2 \rightarrow ZnS + 2AcH \tag{3}$$

Equation 1 represents the formation of primary radicals from the ultrasound-initiated dissociation of water. Equations 2−4 represent the main reactions leading to the formation of ZnS nanoclusters. The formation of H_2S via reaction 2, which has already been suggested by Grieser,[13] further reacts with $Zn(Ac)_2$ to yield ZnS. The freshly generated ZnS nanoclusters interact with the SiO_2 carriers in the reaction medium and form a ZnS-capped SiO_2 composite.

To gain more knowledge about the mechanism of the surface synthesis of ZnS on silica, we have carried out a control experiment, i.e., the sonication of zinc acetate (600 mg) and silica (100 mg) in water, without any sulfur source, under similar sonochemical conditions. The sonication product of zinc acetate−silica (ZAS) was washed repeatedly with water and ethanol and dried in a vacuum. The EDX profile of the ZAS shows the presence of Zn apart from the silica (Figure 8). From the EDX spectrum of ZAS, it is clear that the silica is functionalized with the zinc. The calculated amount of Zn element was ~16%. An attempt that was made to implant Zn on silica, using other salts such as zinc chloride, zinc nitrate, and zinc percholorate, was unsuccessful. Thus we believe that the acetate ligand plays an important role in the grafting of zinc onto silica.

The IR spectra of the ZAS provides evidence for the attachment of zinc through acetate ligands onto silica.

(23) Khosravi, A. A.; Kundu, M.; Jatwa, L.; Deshpande, S. K. Bhagwat, U. A.; Sastry, M.; Kulkami, S. K. *Appl. Phys. Lett.* **1995**, *67*, 2702.
(24) Cizeron, J. Pileni, M. P. *J. Phys. Chem.* **1997**, *101*, 8887.
(25) Becker, W. G.; Bard, A. J. *J. Phys. Chem.* **1983**, *87*, 4888.
(26) Kroger, F. A.; Vink, H. J. *J. Chem. Phys.* **1954**, *22*, 250.
(27) Hayes, D.; Micic, O. I.; Nenadovic, M. T.; Swayambunathan, V.; Meisel, D. *J. Phys. Chem.* **1989**, *93*, 4603. Swayambunathan, V.; Hayes, D.; Schmidt, K. H.; Liao, Y. K.; Meisel, D. *J. Am. Chem. Soc.* **1990**, *112*, 3831.

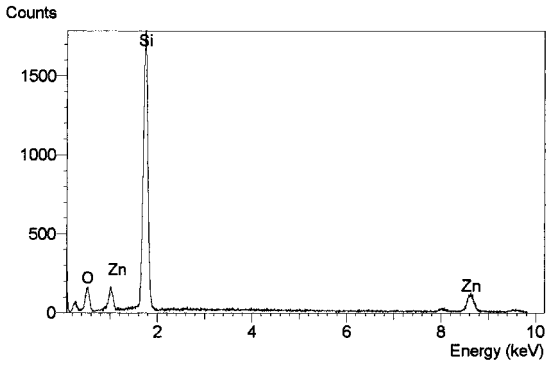

Figure 8. EDX profile of ZAS.

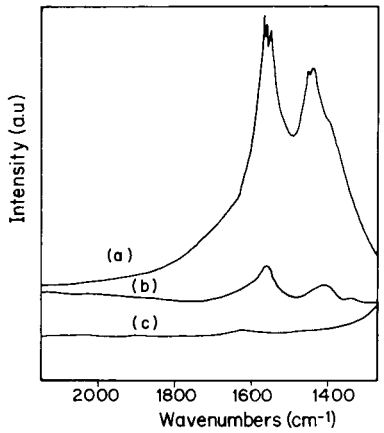

Figure 9. FT-IR spectra: (a) $Zn(ac)_2$, (b) ZAS, and (c) SiO_2.

The IR spectrum of silica and zinc acetate has also been included for comparison in Figure 9. The zinc acetate shows (Figure 9a) two strong absorptions at 1570 and 1450 cm^{-1}, corresponding to the antisymmetric and symmetric stretching vibrations of the COO^- group, respectively. The antisymmetric deformation vibration of the CH_3 group absorbs also in the vicinity of the symmetric stretching COO^-, i.e., 1380−1430 cm^{-1}.[28] On the other hand, the pure silica did not show IR absorption in this region (Figure 9c). The ZAS shows (Figure 9b) a relatively less intense absorption at around 1560 and 1400 cm^{-1}. There is no significant change in the antisymmetric stretching vibration of the COO^- group, even after it is adsorbed on silica. On the other hand, it is clear that the vibration peaked at 1450 cm^{-1}, in ZAS, is shifted toward a lower wavenumber by 50 cm^{-1}. This is explained by us in the following way. The 1450 cm^{-1} band is affected, because it carries some oscillator strength of the CH_3 antisymmetric deformation vibration, and it is likely that there is an interaction between the zinc acetate (solute) and silica via the CH_3 moiety of the acetate group. Such a kind of CH_3 activation by proton abstraction from solute molecules, i.e., formation of $^{\bullet}CH_2$ radicals in sonochemistry, has been well-established.[27] The formation of $^{\bullet}CH_2COO$ radicals ($^{\bullet}Ac$) in various transition metal acetates, in an appropriate liquid medium, has been known in the literature.[29] Accordingly, the formation of solute radicals under sonochemical conditions can be written as:

$$(CH_3COO)_2Zn))))\ (^{\bullet}CH_2COO)_2Zn + 2H^{\bullet} \quad (4)$$

The solute radicals formed under the sonochemical conditions can easily react with reactive surface silica species (siloxanes and silanols), thereby yielding metal-implanted silica.

Therefore, the sonochemical implantation of Zn^{2+} into silica can be visualized in two ways: (i) the reactivity of surface silanol groups (−OH) and solute radicals [This is a consequence of the acidic nature of the silica, the negative polarity of Si−O bonds, and the reactivity of its hydroxyl groups, which allows for an effective interaction with sonochemically formed $Zn(Ac)_2$.] and (ii) the chemical reactivity of $Si-O^-$ nucleation sites formed by the ultrasonic breakage of the strained siloxane link toward the solute radicals, as illustrated in Schemes 2 and 3, repectively. The breakage of the strained siloxane link by ultrasonic cavitation seems to be energetically preferable because it allows the reduction of the structural tensions in this fragment (Si−O−Si), owing to the greater length and lower rigidity of the free Si−O bond.[30]

The zinc acetate implanted into the silica surface then undergoes ligand exchange, with sulfide ions generated according to eq 3, yielding ZnS coated on silica (Scheme 4). Once the surface ZnS is formed, this can act as a nucleating site for the further adhesion of ZnS formed in the bulk solution.

There are several reports on the implantation of transition metal ions on silica surfaces (functionalized silica) by using simple metal salts or organometallic complexes. Voort and co-workers[31] have prepared vanadium implanted into silica by using $VO(AcAc)_2$ in a nonaqueous solvent, as well as in the gas phase. They have suggested that the implantation takes place via the irreversible adsorption of the complex by hydrogen bonding or by a ligand-exchange mechanism. Rice and Scott[32] have immobilized V−Ti alkoxide on silica using an nonhydrolytic route. The dispersed phase is anchored on the silica support as pseudotetrahedral monomers via oxygen bridges. A variety of transition metal *N*,*N*-dialkylcarbamato complexes have been used as precursors for the chemical implantation of metal ions on oxidic silica supports.[33] The advantage of using these ligands is that they contain metal−oxygen (M−O) bonds and are readily attacked by proton-active substances of even moderate acidity. A similar kind of bonding interaction is also possible in zinc acetate and silica, forming ZAS.

5. Conclusion

Luminescent ZnS-capped SiO_2 composite has been successfully accomplished by the simultaneous sonochemical formation of ZnS and its deposition on a SiO_2 surface under ambient conditions. TEM studies on the ZSS composite have revealed strong adhesion, a well-dispersed nature, and uniform coating of the ZnS on the

(28) *Infrared Spectra of Inorganic and Coordination Compounds*; Nakamoto, K., Wiley: New York, 1963; p 198.
(29) Norman, J. A.; Thomas, C. B.; Burrow, M. J. *J. Chem. Soc., Perkin Trans I.* **1995**, 1087.
(30) Pelmenschikov, A. G.; Morosi, G.; Gamba, A. *J. Phys. Chem.* **1991**, *95*, 10037.
(31) Voort, P. V. D.; White, M. G.; Vansant, F. *Langmuir* **1998**, *14*, 106.
(32) Rice, G. L. Scott, S. L. *Chem. Mater.* **1998**, *10*, 620.
(33) Abis, L.; Amico, D. B. D.; Busetto, C.; Calderazzo, F.; Caminiti, R.; Ciofi, C.; Garbassi, F.; Masciarelli, *J. Mater. Chem.* **1998**, *8*, 751.

Scheme 2

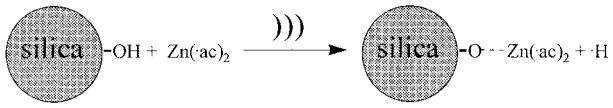

Scheme 3

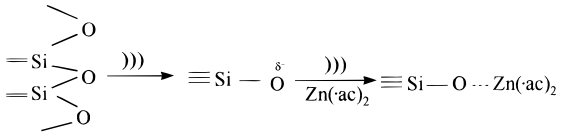

Scheme 4

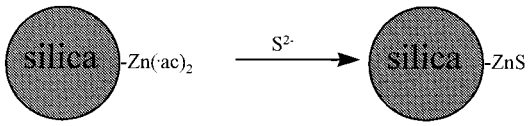

SiO_2 surface as a thin layer or clusters, depending upon the reactant concentrations. FT-IR absorption spectroscopy studies on ZSS composite demonstrate that the amorphous SiO_2 undergoes structural reorganization (breakage of strained siloxane links), followed by the formation of new interfacial linkage upon sonochemical deposition of ZnS. The absorption spectra of sonochemically generated ZnS shows the unusual surface state absorption in the visible region. The surface state absorption detected in ZnS completely disappears in ZSS, probably due to the strong interaction between the core and shell. The absorption edges of ZnS in bare ZnS and in the ZSS are significantly blue-shifted, confirming the quantum effect. The photoluminescence spectra of bare ZnS and ZSS powders demonstrate the quantum size effect. A possible mechanism involving the grafting of zinc acetate onto silica followed by the ligand replacement yielding ZSS, has been proposed. Evidence for the formation of zinc-functionalized silica has been established by EDX and FT-IR studies. The simultaneous use of ultrasound-induced cavitation to generate semiconductor nanoparticles and to activate the carrier surface may be applicable in the surface synthesis of a wide variety of technologically important core/shell-type materials.

Acknowledgment. We thank the Ministry of Science and Arts, Israel, for an Infrastructure grant. We thank Prof. Deutsch and Prof. Erhenberg, from the Department of Physics, and Prof. Malik, from the Department of Life Sciences, for extending their facilities to us. Thanks to Mr. Yitzhak Mestai, from the Weizmann Institute of Science, for his help in band gap calculations. The authors thank Dr. Shifra Hochberg for editorial assistance. A.G. thanks also the NEDC Organization, Japan, for a grant supporting this research.

CM980670S